2016 American Control Conference (ACC)
Boston Marriott Copley Place
July 6-8, 2016. Boston, MA, USA

Chained formulation of 3D path following for nonholonomic autonomous robots in a Serret-Frenet frame

Ali Oulmas[1,2], Nicolas Andreff[2] and Stéphane Régnier[1]

Abstract— **The problem of 3D path following of nonholonomic systems in closed-loop is addressed. The kinematic model in a local coordinate system using a Serret-Frenet frame with sideslip and attack angles is used to express the motion of the robot. A new derivation of the chained form with five states and three inputs is developed to linearize the kinematic model of the robot in order to design a decoupled stable controller. The 3D path following is validated experimentally using a magnetic helical swimmer with visual servo control by following first a helix trajectory then an inclined sinusoidal trajectory. The results show the accuracy and robustness of the controller.**

I. INTRODUCTION

Three-dimensional autonomous robots with nonholonomic constraints such as autonomous underwater vehicles (AUV) and some unmanned aerial vehicles (UAV) are extremely efficient and flexible. Hence, they present solutions to complex or dangerous tasks [1]. For most of these applications, the nonholonomic systems need to follow a desired path to reach a specific location to observe and perform tasks. Two classic kinematic control paradigms exist: trajectory tracking and path following.

This paper focuses on path following because in the presence of disturbances it presents better performance with regard to accuracy and smoother convergence to the path [2]. Indeed, in trajectory tracking, perturbations result in many undesired effects, essentially due to time delays. To overcome this problem, the trajectory tracking tends to compensate the delay by speeding up the velocity of the robot (limited by actuator constrains that impose a saturation on the velocity amplitude) or cutting the trajectory (reduced motion precision). On the other hand, the path following method allows for more precise motion by following the path without any time specification.

In the literature, many researchers demonstrated a 3D path following of nonholonomic autonomous robot in closed-loop. For instance, [3] proposed to use backstepping techniques with Lyapunov theory for the path following of an AUV in space. A recent filtered backstepping control is used in [4] for the path following of a model-scaled autonomous helicopter in order to overcome the drawback of singularities in space. Sliding mode techniques are also used in [5] for an underwater vehicle. These techniques have been shown to be simple and robust against uncertainties. Another approach using the chained system with continuous state feedback law is used in [10] for the planar path following of mobile robots. This approach was extended to an underwater autonomous robot using an H-2 optimal controller for trajectory tracking in [6]. However, because the robot kinematics were expressed in a global frame, this linear time-varying (LTV) controller is not fully decoupled, and the controllability analysis was provided only for the case of constant velocity.

The first contribution in this paper is to describe the system in a local coordinate system using the Serret-Frenet frame with sideslip and attack angles instead of the global frame. The desired motion is thereby expressed in terms of the path parameters (curvilinear abscissa, curvature, torsion ...). The second contribution is to extend [10] to 3D noholonomic autonomous systems with five states and three inputs to design a stable and decoupled controller for 3D path following. The model in [10] will become a subset of our general form and according to [6], the proposed controller is decoupled and linear time invariant (LTI) and the velocity does not affect the control. In addition, the control takes into account the weight of the robot and lateral disturbances.

This approach was validated in experiments using a wireless helical swimmer actuated magnetically by following different curves (a helix trajectory and an inclined sinusoidal trajectory) in space (namely, in a viscous fluid).

This paper is organized as follows: Section II describes the 3D error kinematic model of the robot in a local frame with sideslip and attack angles. Section III details the conversion of the system into the chained form and the control law that allows the path following. Section IV shows the magnetic manipulation system used to steer the swimmer wirelessly. Section V shows the experimentation results obtained by applying the 3D control on the prototype.

II. KINEMATIC MODEL IN THE SERRET-FRENET FRAME OF AN AUTONOMOUS MOBILE ROBOT IN SPACE

To control the autonomous robot, a model describing its behavior is necessary. Therefore, an error kinematic model with the Serret-Frenet frame associated to the reference path is used to express the desired motion in terms of the path parameters. The nonholonomic constraints are also considered.

The kinematics of the autonomous robot with nonholonomic constraints are in general developed using an absolute global frame $\mathbf{U} = \{ \mathbf{x} \ \mathbf{y} \ \mathbf{z} \}$ with origin $\mathbf{O}$ and a moving

*This work was supported by Région Franche-Comté and the French Agence Nationale de la recherche, through the ANR LEMA and ANR Labex ACTION.

[1]A. Oulmas and S. Régnier are with Institut des Systémes Intelligents et Robotique, University Pierre & Marie Curie, 75005 Paris, France ali.oulmas@isir.upmc.fr, stephane.regnier@upmc.fr

[2]A. Oulmas and N. Andreff are with FEMTO-ST Institute, CNRS/University of Franche-Comté/ENSMM/UTBM, 25000 Besançon, France nicolas.andreff@femto-st.fr

body frame $\mathbf{B_r} = \{\ \mathbf{x_B}\ \ \mathbf{y_B}\ \ \mathbf{z_B}\}$ attached to the body of the robot located at **G** the center of mass of the robot (Fig. 1). The orientation of the robot is characterized by the inclination angle θ_i and the direction angle θ_d. The former is the angle between the horizontal plane **xOy** and the axis of the robot and the latter is the angle between the vertical plane **zOx** and the axis of the robot. The rotational velocity of the frame $\mathbf{B}_r$ is ${}^{\mathbf{B_r}}\omega_{\mathbf{B_r}} = [\ \Omega_x\ \ \Omega_y\ \ \Omega_z\ ]$.

In order to compensate the weight of the robot and lateral deviations caused by several external disturbances such as wind, swell or fluidic current, the so-called wind frame $\mathbf{W}=\{\mathbf{x_w}\ \ \mathbf{y_w}\ \ \mathbf{z_w}\}$ is introduced [7]. The total linear velocity v of the robot is defined as the linear velocity along the $\mathbf{x_w}$ axis of the wind frame **W** which is given as:

$$v = \frac{1}{C\alpha C\beta}\, v_p \tag{1}$$

where α and β are respectively the sideslip and attack angles while v_p is the propulsion velocity along the robot axis $\mathbf{x_B}$. Thus, the linear velocity of **W** is ${}^{\mathbf{W}}\mathbf{v_W} = [\ v\ \ 0\ \ 0\ ]^T$. The rotation matrix from **W** to $\mathbf{B}_r$ corresponds to the sequence of rotation $(-\beta,\alpha,0)$ and is given by [8]:

$${}^{\mathbf{B_r}}\mathbf{R_W} = \begin{bmatrix} C\alpha C\beta & -C\alpha S\beta & -S\alpha \\ S\beta & C\beta & 0 \\ S\alpha C\beta & -S\alpha S\beta & C\alpha \end{bmatrix} \tag{2}$$

For ease of notation, we defined $C\cdot = \cos(\cdot)$, $S\cdot = \sin(\cdot)$ and $T\cdot = \tan(\cdot)$.

The path to be followed is denoted by $\mathscr{C}(s)$ which is described with the curvilinear coordinate s, the curvature and torsion of the path being respectively c and τ. $\mathbf{F}=\{\mathbf{x_F}\ \ \mathbf{y_F}\ \ \mathbf{z_F}\}$ is the Serret-Frenet frame that moves along the path $\mathscr{C}(s)$. $\mathbf{x_F}$ and $\mathbf{y_F}$ are respectively tangent and normal to the path while $\mathbf{z_F}$ represents the binormal to the path and is given by the cross product of $\mathbf{x_F}$ and $\mathbf{y_F}$. **F** is characterized by the reference direction angle θ_{dc} and the reference inclination angle θ_{ic} and its linear and angular velocities with respect to the global frame expressed in **F** are given respectively by ${}^{\mathbf{F}}\mathbf{v_F} = [\ \dot{s}\ \ 0\ \ 0\ ]^T$ and ${}^{\mathbf{F}}\omega_{\mathbf{F}} = [\ \tau\dot{s}\ \ 0\ \ c\dot{s}\ ]^T$ [9].

The aim of path following problem is to minimize the distance and orientation errors between the robot and the reference path. For that purpose, the following state vector is defined:

$$\mathbf{q} = \begin{bmatrix} s \\ d_y \\ \theta_{de} \\ d_z \\ \theta_{ie} \end{bmatrix} = \begin{bmatrix} s \\ d_y \\ \theta_d - \beta - \theta_{dc} \\ d_z \\ \theta_i - \alpha - \theta_{ic} \end{bmatrix} \tag{3}$$

where d_y and d_z represent respectively the vertical and horizontal distances between the robot center of mass **G** and the point **S** closest to the path while θ_{de} and θ_{ie} represent respectively the direction and inclination angle errors.

The position ${}^{\mathbf{U}}\mathbf{G_W}$ of the robot in the global frame **U** can be expressed as in Fig. 1:

$${}^{\mathbf{U}}\mathbf{G_W} = {}^{\mathbf{U}}\mathbf{S_F} + {}^{\mathbf{U}}\mathbf{R_F}\,{}^{\mathbf{F}}\mathbf{G_W} \tag{4}$$

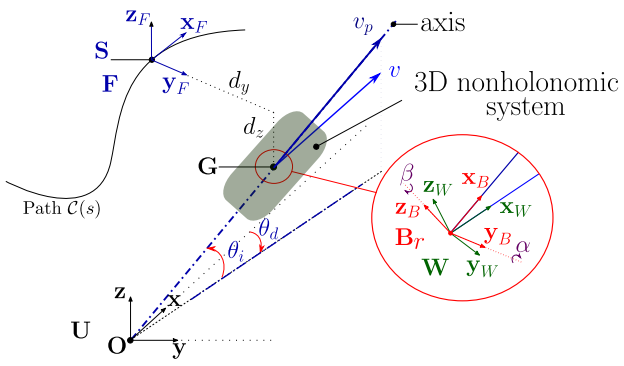

Fig. 1: 3D Path following of a nonholonomic autonomous robot.

where ${}^{\mathbf{U}}\mathbf{R_F}$ is the rotation matrix from **F** to **U** and ${}^{\mathbf{U}}\mathbf{S_F}$ is the closest point on the path expressed in the global frame **U** while ${}^{\mathbf{F}}\mathbf{G_W}$ is the position of the robot in the Serret-Frenet frame and its velocity is hence ${}^{\mathbf{F}}\dot{\mathbf{G}}_{\mathbf{W}} = [\ 0\ \ \dot{d}_y\ \ \dot{d}_z\ ]^T$. Differentiating (4) with respect to the time and expressing it in the Serret-Frenet frame gives:

$${}^{\mathbf{F}}\mathbf{R_W}\,{}^{\mathbf{W}}\mathbf{v_W} = {}^{\mathbf{F}}\mathbf{v_F} + {}^{\mathbf{F}}\dot{\mathbf{G}}_{\mathbf{W}} + {}^{\mathbf{F}}\omega_{\mathbf{F}} \times {}^{\mathbf{F}}\mathbf{G_W} \tag{5}$$

where ${}^{\mathbf{F}}\mathbf{R_W}$ is the rotation matrix from **W** to **F** using Euler angles and is given by:

$${}^{\mathbf{F}}\mathbf{R_W} = \begin{bmatrix} C\theta_{de}C\theta_{ie} & -S\theta_{de} & C\theta_{de}S\theta_{ie} \\ S\theta_{de}C\theta_{ie} & C\theta_{de} & S\theta_{de}S\theta_{ie} \\ -S\theta_{ie} & 0 & C\theta_{ie} \end{bmatrix} \tag{6}$$

The angle rates $\dot{\theta}_{ie}$ and $\dot{\theta}_{de}$ are computed from the relative angular velocity between the Serret-Frenet frame **F** and the frame **W** as follows:

$${}^{\mathbf{F}}\dot{\mathbf{R}}_{\mathbf{W}} = {}^{\mathbf{F}}\mathbf{R_W}\ \mathbf{S}\left({}^{\mathbf{W}}\omega^{\mathbf{r}}_{\mathbf{W,F}}\right) \tag{7}$$

where $\mathbf{S}(\cdot)$ is a skew-symmetric matrix and ${}^{\mathbf{W}}\omega^{\mathbf{r}}_{\mathbf{W,F}}$ is the relative angular velocity which is given as shown in [3] by:

$${}^{\mathbf{W}}\omega^{\mathbf{r}}_{\mathbf{W,F}} = {}^{\mathbf{W}}\omega_{\mathbf{B_r}} + {}^{\mathbf{W}}\omega^{\mathbf{r}}_{\mathbf{W,B_r}} - {}^{\mathbf{W}}\omega_{\mathbf{F}} \tag{8}$$

Solving (5) for $\dot{s}$, $\dot{d}_y$ and $\dot{d}_z$ and (7) for $\dot{\theta}_{ie}$ and $\dot{\theta}_{de}$ gives the following error kinematic model of 3D autonomous robots:

$$\dot{s} = \frac{v\ C\theta_{de}\ C\theta_{ie}}{1 - c\ d_y} \tag{9.a}$$

$$\dot{d}_y = v\ S\theta_{de}\ C\theta_{ie} + \tau\ d_z\ \dot{s} \tag{9.b}$$

$$\dot{d}_z = -v\ S\theta_{ie} - \tau\ d_y\ \dot{s} \tag{9.c}$$

$$\dot{\theta}_{ie} = \Omega_y\ C\beta - \Omega_z\ S\beta\ S\alpha - \dot{\alpha}\ C\beta + \tau\ \dot{s}\ S\theta_{de} \tag{9.d}$$

$$\dot{\theta}_{de} = \Omega_z\ \frac{C\alpha}{C\theta_{ie}} + \frac{\dot{\beta}}{C\theta_{ie}} - \tau\ \dot{s}\ T\theta_{ie}\ C\theta_{de} - c\ \dot{s} \tag{9.e}$$

Note that these equations are not defined at $d_y = \frac{-1}{c}$ and θ_{ie} must differ from $\frac{\pi}{2}[\pi]$.

To check the validity of this model, we calculated the projection of these equations in the horizontal plane setting the variables d_z, τ, α, θ_{ie} and Ω_y to zero, which gave us the

kinematic model used by Samson in [10] and [11] for the planar path following of mobile robots:

$$\begin{cases} \dot{s} &= \dfrac{v\ C\theta_{de}}{1-c\ d_y} \\ \dot{d}_y &= v\ S\theta_{de} \\ \dot{\theta}_{de} &= \Omega_z+\dot{\beta}-c\ \dot{s} \end{cases} \tag{10}$$

III. Chained form and control law

A. Chained form

The total linear velocity v is not aligned with the thrust direction $\mathbf{x_B}$ of the robot because of the weight and lateral disturbances. Therefore, to drive the robot to the path, the total linear velocity v should be aligned with the tangent of the reference path. In other words, the distances d_y and d_z and the orientations θ_{ie} and θ_{de} must be servoed to zero. For that purpose, a stable control law is necessary:

$$(v,\ \Omega_y,\ \Omega_z) \quad = \quad f(d_y,\ d_z,\ \theta_{ie},\ \theta_{de}) \tag{11}$$

The angular velocity Ω_x along the robot axis is not considered because the error in roll does not perturb the path following [3]. The number of inputs is less than the number of degrees of freedom which makes the nonholonomy.

The kinematic model of the autonomous robot formed by (9) is nonlinear. In order to control this kind of system, a solution consists in linearizing it around the equilibrium $d_y = d_z = \theta_{de} = \theta_{ie} = 0$. Samson *et al.* have established an approach to convert the models of planar mobile robots (unicycle, car-like, with trailers) into linear models using chained form with two inputs and three states [10]. The conversion of multi-inputs nonholonomic systems into the chained form is presented in [12] for the fire truck example. Inspired by [11], [12] and [13], we propose to convert the kinematic system of the 3D autonomous robot into the following chained form with three inputs and five states:

$$\dot{x}_1 = u_1 \tag{12.a}$$
$$\dot{x}_2 = x_3\ u_1 \tag{12.b}$$
$$\dot{x}_3 = u_2 \tag{12.c}$$
$$\dot{x}_4 = x_5\ u_1 \tag{12.d}$$
$$\dot{x}_5 = u_3 \tag{12.e}$$

where $\mathbf{x} = (x_1,x_2,x_3,x_4,x_5)^T$ is the state vector and $\mathbf{u} = (u_1,u_2,u_3)^T$ is the input vector. The transformations of (9) into the chained form start by choosing the first variable state as:

$$x_1 \quad = \quad s \tag{13}$$

Thus, from (9.a):

$$u_1 \quad = \quad \dot{x}_1 \quad = \quad \dot{s} \quad = \quad \frac{v\ C\theta_{de}\ C\theta_{ie}}{1-c\ d_y} \tag{14}$$

The input u_1 is a function of the total linear velocity v. Then, the second variable state is chosen as the horizontal distance:

$$x_2 \quad = \quad d_y \tag{15}$$

Thus, from (9.b):

$$\dot{x}_2 \quad = \quad \dot{d}_y \quad = \quad v\ S\theta_{de}\ C\theta_{ie}+\tau\ d_z\ \dot{s} \tag{16}$$

Then, from (12.b), (14) and (16), x_3 is obtained as:

$$x_3 \quad = \quad (1-c\ d_y)\ T\theta_{de}+\tau\ d_z \tag{17}$$

Therefore, from (12.c) yields:

$$\begin{aligned} u_2 &= \dot{x}_3 \\ &= \tau\ \dot{d}_z+d_z\ \dot{s}\ \tfrac{d\ \tau}{ds}+(1-c\ d_y)\ \dot{\theta}_{de}\ (C\theta_{de})^{-2} \\ &\quad -\left(c\ \dot{d}_y+d_y\ \dot{s}\ \tfrac{d\ c}{ds}\right)\ T\theta_{de} \end{aligned} \tag{18}$$

where θ_{de} and θ_{ie} must differ from $\frac{\pi}{2}[\pi]$ and d_y from $\frac{-1}{c}$. Replacing $\dot{s}$, $\dot{d}_y$, $\dot{d}_z$ and $\dot{\theta}_{de}$ by their values in (9), the input u_2 is obtained in function of the steering angular velocity Ω_z:

$$u_2 \quad = \quad \gamma_{21}\ \Omega_z+\gamma_{22} \tag{19}$$

where γ_{21} and γ_{22} are the following scalar variables:

$$\gamma_{21} = (1-c\,d_y)\,C\alpha\,(C\theta_{de})^{-2}\,(C\theta_{ie})^{-1}$$
$$\gamma_{22} = \dot{\beta}\,(1-c\,d_y)\,(C\theta_{de})^{-2}\,(C\theta_{ie})^{-1}$$
$$+\tfrac{v}{-1+c\,d_y}\left(2(1-c\,d_y)\,\tau\,S\theta_{ie}+\left(\tau^2\,d_y-d_z\,\tfrac{d\,\tau}{ds}\right)C\theta_{de}\,C\theta_{ie}\right.$$
$$\left.+\left((-2+C(\theta_{de})^2)\,\tfrac{c\,(c\,d_y-1)}{C\theta_{de}}+(c\,\tau\,d_z+d_y\,\tfrac{d\,c}{ds})\,S\theta_{de}\right)C\theta_{ie}\right)$$

Note that γ_{22} depends on the total linear velocity v of the robot and the derivative of the sideslip angle $\dot{\beta}$.
In the same way, the fourth state variable is chosen as the vertical distance:

$$x_4 \quad = \quad d_z \tag{20}$$

Thus, from (9.d):

$$\dot{x}_4 \quad = \quad \dot{d}_z \quad = \quad -v\ S\theta_{ie}-\tau\ d_y\ \dot{s} \tag{21}$$

From (12.d), (14) and (21), x_5 comes as:

$$x_5 \quad = \quad (c\ d_y-1)\ T\theta_{ie}\ C(\theta_{de})^{-1}-\tau\ d_y \tag{22}$$

Finally, from (12.e) and (22):

$$\begin{aligned} u_3 &= \dot{x}_5 \\ &= -\tau\ \dot{d}_y-d_y\ \dot{s}\ \tfrac{d\ \tau}{ds}+\left(c\ \dot{d}_y+d_y\ \dot{s}\ \tfrac{d\ c}{ds}\right)\ \tfrac{T\theta_{ie}}{C\theta_{de}} \\ &\quad -\left(\dot{\theta}_{ie}\ (C\theta_{ie})^{-2}+\dot{\theta}_{de}\ T\theta_{de}T\theta_{ie}\right)\ \tfrac{1-c\ d_y}{C\theta_{de}} \end{aligned} \tag{23}$$

where θ_{de} and θ_{ie} must differ from $\frac{\pi}{2}[\pi]$ and d_y from $\frac{-1}{c}$. Replacing $\dot{s}$, $\dot{d}_y$, $\dot{\theta}_{ie}$ and $\dot{\theta}_{de}$ by their values in (9), the input u_3 is obtained in function of the steering angular velocities Ω_z and Ω_y:

$$u_3 \quad = \quad \gamma_{31}\ \Omega_y+\gamma_{32}\ \Omega_z+\gamma_{33}. \tag{24}$$

where γ_{31}, γ_{32} and γ_{33} are defined as:

$$\gamma_{31} = (-1+c\,d_y)\,C\beta\,C(\theta_{de})^{-1}\,C(\theta_{ie})^{-2}$$
$$\gamma_{32} = (1-c\,d_y)\,(C\theta_{de})^{-1}\,(C\theta_{ie})^{-2}\left(S\alpha\,S\beta-C\alpha\,S\theta_{ie}\,T\theta_{de}\right)$$
$$\gamma_{33} = (1-c\,d_y)\left(\dot{\alpha}\,C\beta-\dot{\beta}\,S\theta_{ie}\,T\theta_{de}\right)-\tfrac{v\ C\theta_{ie}}{1-c\,d_y}\left(d_y\,C\theta_{de}\,\tfrac{d\,\tau}{ds}\right.$$
$$\left.-d_y\,T\theta_{ie}\,\tfrac{d\,c}{ds}+\left(d_z\,\tau+2\,(1-c\,d_y)\,T\theta_{de}\right)\left(\tau\,C\theta_{de}+c\,T\theta_{ie}\right)\right)$$

Note that γ_{33} depends on the total linear velocity v and the derivatives of the sideslip and attack angles respectively $\dot{\beta}$ and $\dot{\alpha}$.
Now, considering the following change of variables:

$$\forall i = 1,..5, \quad \frac{d}{dx_1} x_i = x_i' \tag{25.a}$$

$$u_{12} = \frac{u_2}{u_1} \tag{25.b}$$

$$u_{13} = \frac{u_3}{u_1} \tag{25.c}$$

The chained form model (12) can be rewritten as:

$$\begin{array}{c} x_1' = 1; \quad x_2' = x_3; \quad x_3' = u_{12} \\ x_4' = x_5; \quad x_5' = u_{13} \end{array} \tag{26}$$

the derivative of x_i with respect to the curvilinear abscissa s defines a system independent of the total linear velocity v of the autonomous robot. Therefore, the control law (11) will be:

$$\begin{array}{rcl} v(t) & = & arbitrary \neq 0 \\ (\Omega_y,\ \Omega_z) & = & f(d_y,\ d_z,\ \theta_{ie},\ \theta_{de}) \end{array} \tag{27}$$

The model (26) is clearly linear and time invariant (LTI) as it can be rewritten:

$$\begin{bmatrix} x_2' \\ x_3' \\ x_4' \\ x_5' \end{bmatrix} = \begin{bmatrix} 0 & 1 & 0 & 0 \\ 0 & 0 & 0 & 0 \\ 0 & 0 & 0 & 1 \\ 0 & 0 & 0 & 0 \end{bmatrix} \begin{bmatrix} x_2 \\ x_3 \\ x_4 \\ x_5 \end{bmatrix} + \begin{bmatrix} 0 & 0 \\ 1 & 0 \\ 0 & 0 \\ 0 & 1 \end{bmatrix} \begin{bmatrix} u_{12} \\ u_{13} \end{bmatrix} \tag{28}$$

B. Control

Therefore, a simple state feedback control law is enough to reach and pursue the reference path:

$$\begin{bmatrix} u_{12} \\ u_{13} \end{bmatrix} = - \begin{bmatrix} k_{d1} & k_{t1} & 0 & 0 \\ 0 & 0 & k_{d2} & k_{t2} \end{bmatrix} \begin{bmatrix} x_2 \\ x_3 \\ x_4 \\ x_5 \end{bmatrix} \tag{29}$$

where k_{t1}, k_{d1}, k_{t2} and k_{d2} are the control gains and are strictly positive. The closed loop performance can be adjusted using these parameters.
Replacing (26) in (29) gives the following equation:

$$\ddot{\mathbf{e}} + \mathbf{K_t}\ \dot{\mathbf{e}} + \mathbf{K_d}\ \mathbf{e} = 0. \tag{30}$$

with:

$$\mathbf{e} = \begin{bmatrix} x_2 \\ x_4 \end{bmatrix}; \quad \mathbf{K_t} = \begin{bmatrix} k_{t1} & 0 \\ 0 & k_{t2} \end{bmatrix}; \quad \mathbf{K_d} = \begin{bmatrix} k_{d1} & 0 \\ 0 & k_{d2} \end{bmatrix}$$

The solution of (30) gives the convergence of both $\mathbf{e}$ and $\dot{\mathbf{e}}$ to zero. After expansion, (30) gives two decoupled 1-dimensional 2^{nd} order systems:

$$\begin{cases} x_2'' + k_{t1}\ x_2' + k_{d1}\ x_2 = 0 \\ x_4'' + k_{t2}\ x_4' + k_{d2}\ x_4 = 0 \end{cases} \tag{31}$$

that independently converge to zero under appropriate gain tuning.
Finally, using (15), (17), (20) and (22) leads to the convergence of the distances d_y and d_z and the orientations θ_{ie} and θ_{de} to zero. Thus, a spatial path following is achieved.

C. Actuation

The linearization gives the following control:

$$\begin{cases} u_2 = \gamma_{21}\,\Omega_z + \gamma_{22} \\ u_3 = \gamma_{31}\,\Omega_y + \gamma_{32}\,\Omega_z + \gamma_{33} \end{cases} \tag{32}$$

By knowing the position of the autonomous robot $\mathbf{G}$ and the path parameters (s, τ and c), the steering angular velocities Ω_y and Ω_z can be computed from (32) as follows:

$$\begin{cases} \Omega_z = (u_2 - \gamma_{22})\ \gamma_{21}^{-1} \\ \Omega_y = \left(u_3 - \gamma_{33} - \gamma_{32}\,\gamma_{21}^{-1}\,(u_2 - \gamma_{22})\right)\ \gamma_{31}^{-1} \end{cases} \tag{33}$$

where the input u_2 is computed using (25.b) and (29) and is given as:

$$\begin{array}{rcl} u_2 & = & -k_{d1}\,u_1\,x_2 - k_{t1}\,|u_1|\,x_3 \\ & = & -k_{d1}\,u_1\,d_y - k_{t1}\,|u_1|\,(\tau\,d_z + (1 - c\ d_y)\,T\theta_{de}) \end{array} \tag{34}$$

In the same way, u_3 is computed from (25.c) and (29) and is given as:

$$\begin{array}{rcl} u_3 & = & -k_{d2}\,u_1\,x_4 - k_{t2}\,|u_1|\,x_5 \\ & = & -k_{d2}\,u_1\,d_z - k_{t1}\,|u_1|\,\big(-\tau\,d_y \\ & & \qquad + (c\,d_y - 1)\,C(\theta_{de})^{-1}\,T\theta_{ie}\big) \end{array} \tag{35}$$

The controller is asymptotically stable when $u_1 = \dot{s}$, the velocity along the path, is constant. Therefore, $\dot{s}$ depends on the total linear velocity v as shown in (9.a). Similar to [11], v has to satisfy certain conditions to ensure the stability: it must be a bounded differentiable time-function, its derivative has to be bounded and $v(t)$ must not tend to zero when t tends to infinity.

As γ_{33} depends on $\dot{\alpha}$ and $\dot{\beta}$, which reflect the variations of the interaction with the environment, the controller also depends on them. Several control strategies can be implemented (that can not be discussed in length in this paper and are not mutually exclusive) including: i) to provide a feedforward estimate; ii) to rely on exteroceptive sensing; iii) to derive an observer similar to the one in [17], which allows for compensating side-slipping in 2D all-terrain control within the framework proposed in [12]; iv) to introduce the associated dynamics in the controller, such as in [18].

In the remainder of this paper, we considered α and β as constant because the experimental environment is rather still and rely on vision feedback for compensating the minor disturbances arising from this choice.

IV. Application to Magnetically Actuated Helical Swimmers

The proposed control law for 3D path following was experimentally tested using a magnetically actuated helical swimmer with 14 *mm* length and 1 *mm* in diameter. Helical swimmers can be considered as autonomous vehicles with nonholonomic constraints, since they advance in direction of their axis by converting the rotary motion into linear motion. However, lateral displacements caused mainly by the boundary effect [14], thermal noise and microfluidic flow are considered as disturbances (similar to the sideslip angle β). Moreover, the apparent weight which is defined as

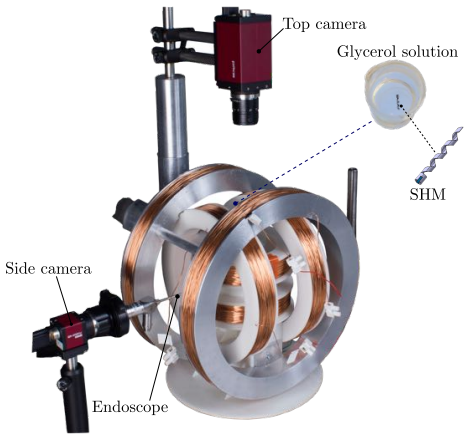

Fig. 2: Magnetic manipulation system

the resultant of the gravity and buoyancy forces is nonzero, thus creates a downward drift defined as the attack angle α in Fig. 1. The closed-loop control aims to correct these disturbances.

In order to wirelessly actuate the helical swimmer in space, a non contact magnetic system composed of three pairs of coils in Helmholtz configuration is used to generate a uniform rotating magnetic field in the center of the workspace (Fig. 2). The magnetic torque $\mathbf{T}$ applied on the helical swimmer is given by:

$$\mathbf{T} = \mathbf{M} \times \mathbf{B} \tag{36}$$

where $\mathbf{M}$ is the magnetic moment of the helical swimmer and $\mathbf{B}$ the magnetic field. The magnetic torque tends to align the magnetic moment with the applied magnetic field. Therefore, with a rotating magnetic field and a helical tail, the helical swimmer can advance by converting the rotational motion into linear motion.

The magnetic field can be decomposed into a magnetic field $\mathbf{B}_\perp$ perpendicular to the helical swimmer axis and a magnetic field $\mathbf{B}_\parallel$ parallel to the helical swimmer axis [15]. The first vector yields the open-loop self-rotation of the helical swimmer and is given by:

$$\mathbf{B}_\perp = B_0 \ \cos(2\pi f t) \ \tilde{\mathbf{u}} + B_0 \ \sin(2\pi f t) \ \tilde{\mathbf{v}} \tag{37}$$

where B_0 is the magnetic flux density in the center of the workspace and $\tilde{\mathbf{u}}$ and $\tilde{\mathbf{v}}$ are the basis vectors of the plane perpendicular to the axis of the helical swimmer.
The second vector yields the steering of the helical swimmer in order to reach the target orientation and can be expressed as [15]:

$$\mathbf{B}_\parallel = -sign(\mathbf{B}_\perp \ \mathbf{n}^*) \ \lambda \ \ \| \mathbf{n} \times \mathbf{n}^* \| \ \mathbf{n} \tag{38}$$

where $\mathbf{n}$ and $\mathbf{n}^*$ are respectively the real-time and desired orientations of the helical swimmer and λ is the control gain. The tuning of this gain is empirical.

The position $\mathbf{G}$ and orientation of the swimmer are reconstructed by stereovision. The helical swimmer axis $\mathbf{n}$ is related to the direction and inclination angles as follows:

$$\mathbf{n} = \begin{bmatrix} S\theta_i & C\theta_i S\theta_d & C\theta_i C\theta_d \end{bmatrix}^T \tag{39}$$

$\mathbf{B}_\parallel$ is thus the "actuator" associated to the steering angular velocities Ω_z and Ω_y in (33), which are related to the desired inclination and direction angles as follows:

$$\begin{cases} \theta_d^*(t) &= \theta_d(t) + \Omega_z \ dt \\ \theta_i^*(t) &= \theta_i(t) + \Omega_y \ dt \end{cases} \tag{40}$$

which is transformed into $\mathbf{n}^*$ thanks to (39).

In the case of helical swimmers, the propulsion velocity v_p is defined thanks to the so-called propulsion matrix [16].

V. Experimental results

In this section, the 3D control developed above is tested on the prototype by following a helix and an inclined sinusoidal trajectories.

A. Helix trajectory

The swimmer rotates in synchronization with the rotating magnetic field at a frequency of $f = 2.6\ Hz$ and was initially placed near the desired path.

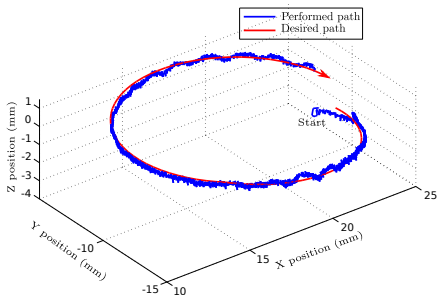

Fig. 3: The 3D reconstruction of the trajectory drawn by the helical swimmer while following a helix trajectory with the control gains of $k_{t1} = 0.004$, $k_{d1} = 0.05$, $k_{t2} = 0.3$

Fig. 3 depicts the result of the 3D reconstruction by vision of the helical swimmer position where the reference path is drawn by a red line and the performed path is in blue. It can be noted that the swimmer follows the helix trajectory despite the curve complexity.

The distance and orientation errors are given in Fig. 4. The distance error d_z is maintained to zero, as well as the inclination orientation error θ_{ie} in Fig. 4.b. However, the distance error d_y is also maintained to zero but the direction orientation error θ_{de} is not zero, as shown in Fig. 4.b.

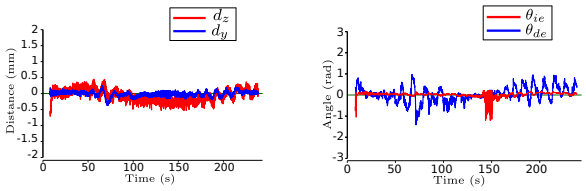

(a) (b)

Fig. 4: Evolution of the distance errors (a) and the orientation errors (b) during the helix trajectory following.

This can be explained by the fact that the environment presents many lateral disturbances. The closed-loop control compensates these disturbances by increasing the direction angle and keeping the lateral error d_y to zero.

A more complicated curve with variable curvature and inclination will be tested in the next section.

B. Inclined sinusoidal trajectory

An inclined sinusoidal trajectory is generated in order to evaluate the controller and the behavior of the swimmer to this kind of path. The swimmer rotation frequency was $f = 3\,Hz$. Fig. 5 depicts the result of the 3D reconstruction

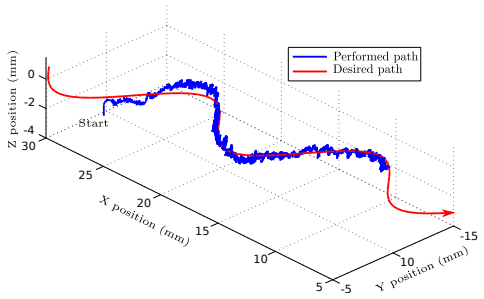

Fig. 5: The 3D reconstruction of the inclined sinusoidal trajectory drawn by the helical swimmer with the control gains of $k_{t1} = 0.04$, $k_{d1} = 0.05$, $k_{t2} = 0.05$ and $k_{d2} = 0.08$.

by vision of the helical swimmer position and compares it to the reference path. The swimmer was initially placed near the desired path. It can be seen that the swimmer follows the path all along despite the succession and complexity of curvatures. The controller is still efficient.

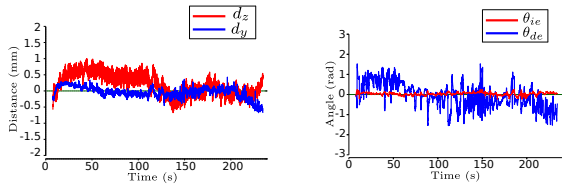

(a) (b)

Fig. 6: Evolution of the distance error d_z (a) and the inclination orientation error θ_{ie} (b).

It is noticed that at the end of the trajectory near the beaker wall, the swimmer is affected by a lateral disturbance, namely the boundary effect [14]. The closed-loop aims to correct this error by increasing the direction angle as shown in Fig. 6.b. To estimate the accuracy, we compute the root-mean-square (RMS) and standard deviation (SD) errors (TABLE I). It can be seen that the accuracy of the path following is submillimetric for both trajectories.

TABLE I: The trajectory errors.

Curves	Errors	d_y (μm)	d_z (μm)	θ_{de} (rad)	θ_{ie} (rad)
Helix	RMS	83.4	199	0.349	0.151
	SD	82.6	189	0.348	0.117
Sinus	RMS	178	396	0.597	0.079
	SD	173	337	0.594	0.068

VI. CONCLUSIONS

A new approach to achieve a 3D path following of a non-holonomic autonomous robot was introduced. The kinematic model of the robot was expressed in a local frame using the Serret-Frenet frame with a new chained formulation to realize the control. The resulting system is decoupled and linear time invariant. The method was validated and analyzed through experimental results using a helical swimmer by following first a helix trajectory and then an inclined sinusoidal trajectory. The results show that the controller is accurate and stable.

REFERENCES

[1] G. Dudek, M. Jenkin. *Computational Principles of Mobile Robotics.* Cambridge University Press, 2010.

[2] L. Lapierre, D. Soetanto and A. Pascoal. *Nonlinear path following with applications to the control of autonomous underwater vehicles.* IEEE Conference on Decision and Control, vol. 2, pp. 1256-1261, 2003.

[3] P. Encarnaao and A. Pascoal. *3D Path Following for Autonomous Underwater Vehicle.* IEEE Conference on Decision and Control, vol. 3, pp. 2977-2982, 2000.

[4] B. Zhu and W. Huo. *3D Path-Following Control for a Model-Scaled Autonomous Helicopter*. IEEE Transactions on Control Systems Technology, vol. 22, pp. 1927-1934, 2014.

[5] A. Healey and D. Lienard. *Multivariable Sliding-Mode Control for Autonomous Diving and Steering of Unmanned Underwater Vehicles.* IEEE Journal of Oceanic Engineering, vol. 18, pp. 327-339, 1993.

[6] S. Wadoo, S. Sapkota and K. Chagachagere. *Optimal Control of an Autonomous Underwater Vehicle*. IEEE International Conference on Systems, Applications and Technology, pp. 1-6, 2012.

[7] T. Oliveira, P. Encarnaao and A. Aguiar. *Moving Path Following for Autonomous Robotic Vehicles*. European Control Conference, pp. 3320-3325, Zrich, Switzerland, 2013.

[8] B. Etkin. *Dynamics of Atmospheric Flight*. Courier Corporation, 2012.

[9] J. Oprea. *Differential geometry and its applications*. The Mathematical Association of America, 2007.

[10] C. Samson. *Control of chained systems application to path following and time-varying point-stabilization of mobile robots*. IEEE Transactions on Automatic Control, vol. 40, no. 1, pp. 64-77, 1995.

[11] P. Morin and C. Samson. *Motion Control of Wheeled Mobile Robots.* In Springer Handbook of Robotics, pp. 799-826, Springer Berlin Heidelberg, 2008.

[12] L. Bushnell, D. Tilbury and S. Sastry. *Steering Three-Input Chained Form Nonholonomic Systems Using Sinusoids: The Fire Truck Example*. Electronics Research Laboratory, College of Engineering, University of California.

[13] G. Walsh, L. Bushnell *Stabilization of multiple input chained form control systems.* Systems & Control Letters, vol. 25, no. 3, pp. 227-234, 1995.

[14] K. Peyer, L. Zhang, B. Kratochvil and B. Nelson. *Non-ideal Swimming of Artificial Bacterial Flagella Near a Surface.* IEEE International Conference on Robotics and Automation, pp. 96-101, USA, 2010.

[15] T. Xu, G. Hwang, N. Andreff and S. Régnier. *Characterization of Three-dimensional Steering for Helical Swimmers.* IEEE International Conference on Robotics and Automation, pp. 4686-4691, 2014.

[16] T. Xu, G. Hwang, N. Andreff and S. Régnier. *Modeling and Swimming Property Characterizations of Scaled-Up Helical Microswimmers*. IEEE/ASME Transactions on Mechatronics, vol. 19, no. 3, pp. 1069-1079, 2014.

[17] R. Lenain, B. Thuilot, C. Cariou and P. Martinet. *Mobile robot control in presence of sliding: Application to agricultural vehicle path tracking.* IEEE Conference on Decision and Control , pp. 6004-6009, 2006.

[18] R. Lenain, B. Thuilot, C. Cariou and P. Martinet. *Mixed kinematic and dynamic sideslip angle observer for accurate control of fast off-road mobile robots.* Journal of Field Robotics, vol. 27, no 2, pp. 181-196, 2010.